RESEARCH ARTICLE

Electroacupuncture Efficacy Evaluation on Blood-Brain Barrier and Cerebral Blood Flow Function in SAMP8 Mice

Zidong Wang[1#], Runquan Sun[2#], and Jiayi Yang[1#], Jing Jiang[1], Yuting Zhang[3], GuoqingWu[1], Yilin Tao[1], Xiaoteng Xu[1], Xiaoyue Zhao[1], Anping Xu[1], Xiaojie Sun[4*] and Zhigang Li[1*]

[1]Department of Acupuncture-Moxibustion and Tuina, Beijing University of Chinese Medicine, Beijing 102488, China; [2]The Sixth Medical Center of the General Hospital of the People's Liberation Army of Chinese, Beijing 100048, China; [3]Experimental Animal Center, Beijing University of Chinese Medicine, Beijing 102488, China; [4]Traditional Chinese Medicine Department. Beijing ShangDi Hospital, Beijing 100084, China
#These authors contributed equally to this work as co-first authors.
*Corresponding author: lizhigang620@126.com (ZL); sunxj0808@foxmail.com (XS)

A B S T R A C T

Insufficient cerebral blood flow plays a pivotal role in neuropathology in humans and animals, producing Alzheimer's disease (AD) like symptoms. Blood brain barrier (BBB) dysfunction may be one of the potential causes of insufficient cerebral blood supply, leading to these problems. Electroacupuncture (EA) can show promise in improving cognitive abilities and CNS functions. However, its effects on cerebral blood flow and the blood-brain barrier are not yet clear. SAMP8 mice were randomly assigned to three experimental groups: the Alzheimer's disease model (AD), electro-acupuncture intervention (EA), and donepezil treatment (D) groups. SAMP8 mice received EA at GV20/GV29 (2 mA, 100/2 Hz) in the EA group or donepezil (1mg/kg) in the D group for 21 days. SAMR1 mice serve as optimal controls for SAMP8 in AD research due to their genetic congruence and age-matched normal aging profile, which effectively isolate AD-specific pathologies by eliminating non-AD-related aging confounders, it worked as the normal (N) controls. Morri's water maze observed the behavioral changes of mice in all groups, the blood flow perfusion in the cortical area of the cerebrum was observed by the RFLSI ZW laser speckle imaging system, and the integrity of the basement membrane and tight junctions of the BBB were observed by transmission electron microscope. Nissl and Hematoxylin and eosin staining observed the morphological changes of nerve cells in the hippocampal region. Cytokine and protein expression levels were determined by Enzyme-Linked Immunosorbent Assay or western blotting. Compared with the N group, cognitive ability and cerebral blood flow were significantly decreased, the function and integrity of BBB were disrupted, the neuronal structure was heavily damaged, and the serum and brain inflammatory responses were increased in mice of the AD group (P<0.01). All of these pathologies were recovered by the EA group and D group (P<0.05/P<0.01). Although the positive control drug donepezil partially ameliorated cognitive deficits, cerebral blood flow (CBF), and neuropathological damage in SAMP8 mice, EA uniquely restored CBF to control levels and exhibited stronger anti-inflammatory effects than donepezil. The results of this study show that EA improves the cognitive ability of mice and alleviates central neuronal damage. This protective effect might be attributed to EA's dual mechanisms of enhancing cerebral perfusion and suppressing inflammatory pathways, mediated through MMp-9 and ICAM-1inhibition, which collectively restore blood-brain barrier integrity and mitigate barrier damage.

INTRODUCTION

Cerebral hypoperfusion and blood-brain barrier (BBB) damage have critical importance in the pathologies of the central nervous system in multiple neurodegenerative diseases (Yang *et al.*, 2020). One of the critical pathophysiological features of BBB pathologies is insufficient cerebral blood flow (CBF), which has been linked to the impairment of the BBB (Feng *et al.*, 2023; Song *et al.*, 2024). The BBB is principally responsible for the maintenance of the ion balance of the brain (CNS). Vascular pathology is concurrent with the mechanisms underlying aging, and brain tumors. However, in AD, the integrity of the BBB is damaged, causing high permeability and subsequent neuronal damage. Dysfunction of the blood-brain barrier (BBB) has become increasingly recognized as the main part of the pathophysiology of neurodegenerative disorders, with studies demonstrating its presence in animal disease with symptoms remarkably akin to those of AD. In humans and animals, BBB breakdown could lead to the accumulation of neurotoxins, impaired clearance of amyloid-beta, and stagnant neuroinflammation, all of which contribute to cognitive decline and memory loss (Liao *et al.*, 2024; Li *et al.*, 2025). Experiments in animals, involving genetically altered mice or artificially damaged BBB mice, have demonstrated Alzheimer's-type pathological features, including the development of amyloid plaques, synaptic dysfunction, and behavioral deficits. Such associations not only highlight the BBB's critical role in cerebral homeostasis but also provide insightful information regarding the pathogenetic mechanisms of Alzheimer's disease, thus presenting potential therapeutic targets as a means to preserve BBB integrity (Luan *et al.*, 2013).

AD is also called senile dementia and it is a set of signs and symptoms because of several pathologies of the CNS, which causes progressive *memory* loss, *cognitive dysfunction*, confusion, and loss of self-consciousness (Whitehouse *et al.*, 1982; Huang *et al.*, 2024) in result of multiple neuropathological events i.e., epilepsy, brain tumor, and elderly degeneration (Reitz and Mayeux, 2014), affecting approximately 50 million people and multiple species of animals although less reported (Botella Lucena and Heneka, 2024; Zhang *et al.*, 2024). Clinical treatments for AD-related neuropathologies have evolved rapidly, including therapies aimed at enhancing brain metabolism, acetylcholinesterase inhibitors, and antioxidant drugs designed to mitigate the accumulation of beta-amyloid plaques and neurofibrillary tangles (NFTs) (Luan *et al.*, 2013). However, clinical trials targeting the elimination of these pathological hallmarks have largely yielded disappointing results (Zhang *et al.*, 2021; Paul *et al.*, 2024). Clinical efficacy remains unsatisfactory, often hindered by adverse effects associated with prolonged use, including an increased risk of cancers (Liao *et al.*, 2024; Li *et al.*, 2025). This highlights the urgent need for more effective and safer therapeutic strategies in the management of AD.

Cerebral ischemia can lead to damage and death of neurons and may trigger the pathological process of AD. For instance, ischemic injury can result in abnormal expression of genes related to AD (Feng *et al.*, 2023).

Such as the accumulation of presenilin 2 gene and β-amyloid precursor protein, these changes are closely related to promoting the inflammatory cascade reaction in the brain, leading to neuronal death and neurodegeneration (Hu and Feng, 2017; Wan *et al.*, 2024). Additionally, cerebral ischemia can also lead to changes in the blood-brain barrier, further exacerbating the accumulation of neurotoxic substances (such as β-amyloid protein) (Li *et al.*, 2025). BBB impairment is considered an early biomarker of AD (Huang *et al.*, 2024). BBB dysfunction can promote the entry of toxic components such as amyloid-β (Aβ) and tau protein into the brain parenchyma, triggering inflammatory responses and neurodegeneration. Studies have also found that the damage to the BBB is closely related to the pathological features of AD, such as Aβ deposition and tau protein hyperphosphorylation. Pro-inflammatory cytokines like TNF-α, IL-8 disrupt endothelial tight junctions by downregulating ZO-1/Occludin (Virgintino *et al.*, 2004; Zhang *et al.*, 2022).

Persistent low-intensity central inflammation is a controllable risk factor in the initial stages of AD (Weijie *et al.*, 2024). The first biological changes of patients begin decades before the first clinical symptoms, and the inflammatory reaction is even earlier than the formation of AD senile plaque, so central inflammation can be used as an early warning of AD. AD-related pathological products can also be detected in the peripheral serum of patients with AD, suggesting that there may be a close relationship between the periphery and the center (Kacířová *et al.*, 2020). The treatment of AD focuses on symptom relief. Cholinesterase inhibitors (such as donepezil) and NMDA receptor antagonists have limited efficacy and do not explain the underlying pathophysiological mechanisms. However, donepezil is still the first-line drug in AD clinical treatment and can be used for positive control.

As a supplementary replacement therapy, acupuncture has a multilayered and multiphasic therapeutic effect (Zhang *et al.*, 2021; Dai *et al.*, 2024). Our previous research showed that electroacupuncture (EA) was effective in improving the cognitive ability of AD mice, which could inhibit the excessive activation of microglia, increase the absorption of glucose in the hippocampus and promote the microcirculation metabolism in the relevant brain regions, repair neurovascular unit dysfunction in AD (Ding *et al.*, 2020). EA's ability to modulate neurovascular coupling and inflammatory pathways positions it as a potential therapy for BBB repair. This study is intended to evaluate the possible beneficial effects of EA on AD by the enhancement of blood supply to the AD-affected degenerated tissues.

MATERIALS AND METHODS

Experimental animal: The senescence-accelerated mice prone-8 (SAMP8), and cognate normal senescence-accelerated mice -R1(SAMR1), which were derived from the SAM-P/2 line by Takeda as a mouse model for increasing neuropathologies producing (dementia) mouse model, with the pathological characteristics related to senescence spontaneous senescence in short life span,

progressive dementia and Aβ deposition, which provides a reliable animal model for AD study (Takeda *et al.*, 1997). All the specific pathogen-free male mouse strains were purchased from the Beijing Zhongke Zesheng Science and Technology [Animals Lot: SCXK (Jing) 2014-003]. The mice of all the groups had an average weight of about (26±2) g and were 7.5 months old. They were raised in a single cage within the animal room of a barrier environment, where the IVC (Individually Ventilated Cage) system ensures a clean environment during the feeding stage and provides feed for Specific Pathogen Free-level experimental mice.

Adaptive feeding for a week before the experiment. Room humidity 40%-70%, and a temperature of 22±2°C, under a 12h dark/light cycle. All experimental procedures complied with the guidelines of the Principles of Laboratory Animal Care formulated by the National Institutes of Health and the legislation of the People's Republic of China for the use and care of laboratory animals. The experimental protocols were approved by the Medicine and Animal Ethics Committee of the Beijing University of Chinese Medicine (Animal Ethics Review Number: BUCM-4-2022102001-4022).

Intervention and grouping methods: Thirty-six male SAMP8 mice were randomly distributed into three groups: An electroacupuncture group (EA), the Donepezil group (D), and the AD model group (AD). Male SAMR1 mice were used as the normal control group (N) (n=12). The experiment includes two major parts: in vivo and in vitro experiments, and the overall process is shown in Fig. 1.

EA group: During the experimental handling, the mice were kept in hand-made mouse bags, while the mouse restraint device was used only during brief electroacupuncture operations and will not affect the long-term feeding conditions. The needles were transversed, puncturing into the point of mice GV20 (Baihui) andGV29(Yintang) at a penetration of 2-3 mm with sterile disposable acupuncture needles with specifications of (0.25mm×13mm, Beijing Zhongyan Taihe Med. Co. Ltd). GV26 mice were treated with the pricking method and needles were not retained.

The handle of the needles was attached to the HANS-LH202 electroacupuncture device, with a sparse wave at one hundred/2Hz, 2V, and 2mA. The appropriate intensity of EA was the microtremor of the animal head. The period of EA and acupoints selection s was based on results from our previous experiments (Ding *et al.*, 2020). Administration of EA was done for a time of 20 minutes simultaneously.

Daily for 3 weeks, Drug Group of mice (D): Tablets of Donepezil hydrochloride (Eisai China Incorporation Sr: H20050978) were given by intragastric administration at a dose of 1mg/kg (Xiao *et al.*, 2020). AD model group (AD) and mice group normal control (N) were not given any treatment under the same feeding conditions. The mice in the above groups were operated on once daily for 21 days. Simultaneously with the intervention of the EA group, other groups were bound with the same size mouse bags for 20 minutes/day to ensure that the external treatment conditions were the same.

Morris water maze behavior experiment
Hidden platform trial: After 21 days of intervention, the mice in all groups were treated with the Morris water maze hidden platform assay for detection of their spatial learning ability. It is carried out in a circular pool (diameter:120cm, height:50cm). Different solid shapes were affixed to the boundaries of the four quadrants of the pool wall to mark the spatial location of the mice. In the center of the northeast corner of the pool, a platform (diameter:9.5cm, height:28cm) was placed on a circular top to keep the position fixed. The water was added to the surface 2cm higher than the provided platform, and temperature was controlled at (22±1) °C. The camera above the pool is connected to the image acquisition system, and the software system records experimental indexes in real time. Each mouse was randomly put into the pool from different quadrants and were given 60 seconds to find the hidden platform. When the mice climbed onto the platform and stayed for more than 3 seconds, the system automatically saved and recorded the data before the mice found the platform. If the platform cannot be found within 60 seconds, the operator guides the mouse to rest on the platform for 10 seconds, and the escape incubation period is recorded as 60 seconds. Four times in 24 hours were consecutively performed for 5 days.

Probe trial experiment: Probe trial was conducted on day 6. Each mouse was put into the water from the opposite side of the original platform quadrant once for 60 seconds, and the swimming distance of each group in the target quadrant (original platform quadrant) and the ratio of swimming distance to the total distance in the original platform quadrant were recorded as an index of reference memory.

RFLSI ZW laser speckle imaging LSI: On the day following the water maze experiment, the mice were anesthetized with gas (the induction concentration of isoflurane was 2.5%, and the maintenance concentration was 1.5%). Subsequently, the mice were fixed onto the apparatus, and their body temperature was controlled at 37.0±0.5°C by a direct-current feedback heating blanket (produced by FHC Inc., Bowdoinham, USA) to prevent death resulting from hypothermia during the anesthesia process. The scalp of the mice was cut open using medical scissors, the tissues on the skull were removed to expose the visual field of the cerebral cortex, and glycerol was dripped onto the opened area to alleviate the reflection of incident light. During the experiment, the integrity of the mice's skulls and the tissues beneath the skulls was maintained, which could guarantee long-term observation of the experimental mice and also reduce the errors that might be caused by heartbeat and respiration. The RFLSI ZW laser speckle imaging system was turned on, its parameters were adjusted (Exposure time:20ms, Filtering constant: 3s, Algorithm mode: Spatial algorithm (Sliding mode), Frame rate:1.00fps (interval time 00:00:01), Background threshold:10, Pseudo color image resolution:1032x772, working distance:160mm.), and the cerebral blood flow perfusion volume of mice in all groups was measured.
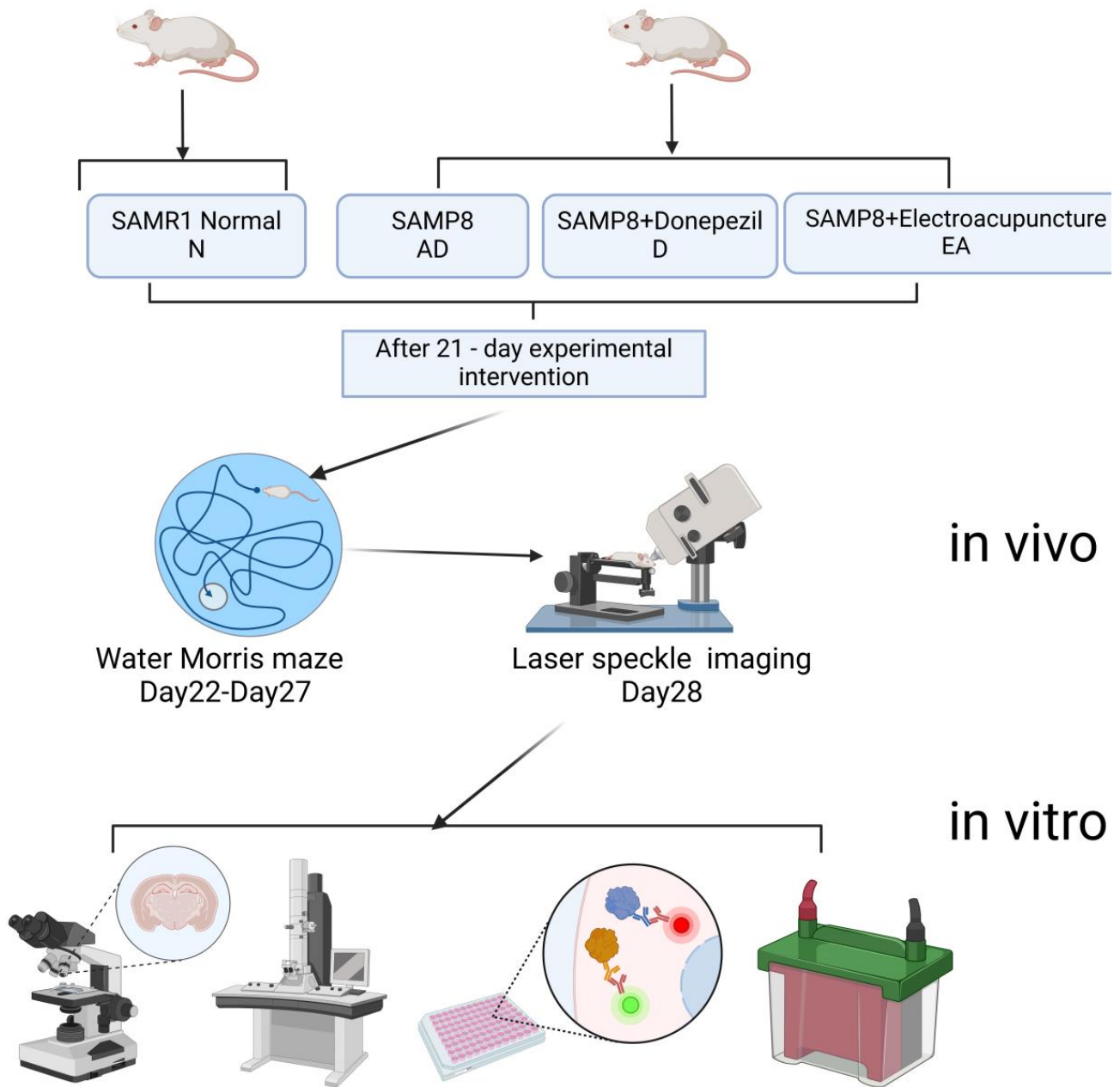
Fig. 1: Flow chart describing the experimental design.

HE and Nissl stain: Three mice in every group were selected randomly, and the mice brain tissues were fixed, embedded, sliced, stained, and sealed according to the routine HE and Nissl staining procedure. The cellular morphology of cells of the hippocampal CA3 region was visualized in the light microscope under different magnifications, and the visual field of the hippocampal CA3 region was randomly taken in each group.

Transmission electron microscope: The dissected mouse brain, immediately fix it with a 3% glutaraldehyde solution for 4 hours and then was sectioned (1 x 1 x 1 mm³) (Yang *et al.*, 2022). Postfixed samples were incubated in 1% osmium tetroxide and dehydrated at room temperature in a gradient series of acetone concentrations. The samples were fixed in EPON/812 resins and then sectioned into 60-nanometer-thick slices using an ultramicrotome. The ultrathin sections are stained twice with uranyl acetate and lead citrate and then

evaluated and photographed using a transmission electron microscope (Microscope HT7800 Series, Japan).

Enzyme-linked immunosorbent assays (ELISA): After intraperitoneal injection anesthesia of the mice (1.25% avertin, 0.2 mL/10g), the whiskers of the mice were cut off, and hematological specimens were taken by eyeball extraction. Subsequently, the mice were slaughtered by dislocation of the cervical joint. The brain tissue was rapidly removed under low-temperature conditions. The hippocampal tissue was isolated and kept in tubes used for cryopreservation and then stored in a -80℃ cryopreservation chamber until taken out for testing. The centrifuge tubes were centrifuged at a temperature of 4℃ and 10,000 rpm for 15 minutes. The serum was taken and which was then placed in a cryopreservation tube and storage at -20 was done until taken out for testing. The content of proinflammatory factors Il-10 and TNF-α(proteinates) in the hippocampus and serum (dilution of

1:5 concentration of dilution) was used respectively, and all the steps were performed according to the instructions of the kit.

Western blotting analysis: Take out tissue from -80°C, weigh 50mg into 1.5mLEP tube, and add protein lysate of 1mL and put tissues of mice in each group into automatic homogenizer for homogenization and break up, and then 30min into 4°C to decompose. Tissues were centrifuged at 4°C and 13,000 revolutions per minute for 15 minutes. The concentration of proteins was estimated with BCA protein test kits. Prepare SDS denatured 10% polyacrylamide gel and SDS denatured 5% polyacrylamide gel. Protein electrophoresis was carried out by adding SDS-PAGE gel to the pores. At the first constant voltage of 80V, the sample runs to the dividing line between the concentrated glue and the separation gel, and when pressed into a straight line, the voltage is adjusted to 120V until the bromophenol blue runs out, and the electrophoresis can be terminated. Protein specimens were dissolved in a buffer and heat-denatured for 10 minutes before separation by SDS-PAGE and electro-transferring on the PVF membrane. The PVF membrane was jammed with blocking buffers for western blot assay and subsequently treated overnight with the corresponding primary antibody. The secondary antibody and membrane were incubated at room temperature for 2h, and protein bands were detected with a Tanon Imaging System.

Statistical analysis: The statistical data were processed by SPSS26.0(USA)software, and all data were expressed by mean ±standard deviation (x±s). The escape latency of the Hidden platform test and swimming speed results were analyzed by multivariate analysis of the variance of repeated measurement. One-way ANOVA was utilized alongside other data. In the test for homogeneity of variance, if $P>0.05$, a pairwise comparative analysis was conducted using the LSD method. When $P<0.05$, pairwise comparisons were made with Tamhane's T2 method. For data that is not normally distributed or has unequal variances, the Kruskal–Wallis test was applied. Statistical significance was established at $P<0.05$, whereas a higher significance level was defined as $P<0.01$.

RESULTS

EA stimulation improved the learning and memory capabilities of mice:
Hidden platform trial: The findings of the MWM test are shown in Fig. 2. Except for the AD group, the movement trace of the search platform for the other groups exhibited a transition from disordered to purposeful searching. On the first day, there was anon significant difference in escape latency between SAMP8 mice and SAMR1 mice. The escape latency of the N, D, and EA groups decreased gradually from day 2 to day 5 and lowered significantly from the 3rd-5th days ($P<0.05$/$P<0.01$). From the second day onwards, the escape latency of the N group significantly decreased compared to the AD group mice ($P<0.01$). The latency of escape in mice of EA and D groups was severely less than mice in the AD group on days 3rd to 5th and days 4-5,

correspondingly ($P<0.05$/$P<0.01$). On a specific day, groups EA and D were not significantly different in their escape latency period in comparison to the groups N mice. However, throughout the hidden platform, the latency to escape of the D group mice was more than N group mice ($P<0.05$), and there was no significant difference between EA and N ($P>0.05$). No significant differences were observed between the EA group mice and D group mice. There was no significant difference in swimming speed among groups (Fig. 2b).

Probe trial: In the probe trial, the number of platform crossovers and the distance of swimming in the northeast portion, where the hidden platform was located, of the AD group were significantly less than mice of group N ($P<0.01$). The platform crossover numbers and the distance of swimming in the northeast of the D and EA mice were significantly higher than those of the AD mice ($P<0.01$). Compared with the N group, these were drastically lower than that in the D and EA groups ($P<0.01$/$P<0.05$). Nonsignificant differences were found in the EA and D groups ($P>0.0$) (Fig. 2c, d).

Mouse swimming traces: The ways for mice to find a platform can be divided into different types: random type, marginal type, trend type, and linear type. Different search types often represent that mice look for platforms with different strategies. The swimming trace of N, D, and EA group will show the change of marginal type and random type to trend type or linear type from day 1-day 5 (Fig. 2e). However, it is difficult to find the law of purposeful search for the platform position in the swimming traces of the AD group, whose traces were mostly random or marginal (Fig. 2e).

EA and donepezil improved the regional cerebral blood flow of SAMP8 mice: Ischemia in the brain can result in neuronal harm and mortality, possibly setting off the pathological progression of Alzheimer's disease (Ułamek-Kozioł et al., 2020). To explore whether the improvement of cognitive damage by EA and donepezil stimulation is related to brain ischemia, we used a laser speckle imager to collect the CBF in each group of mice. We found that in comparison to the N group, the AD mice had a significant decrease in CBF ($P<0.01$) and the presence of a cerebral ischemia phenomenon. However, the D group and the EA group could significantly improve the CBF compared with the AD group ($P<0.05$ or $P<0.01$). However, compared with group N, group D remained at a lower level of CBF（$P<0.01$）, while there was no significant difference between group EA and group N（$P>0.05$）. In addition, the CBF perfusion in group EA was significantly higher than that in group D ($P<0.01$) (Fig. 3).

EA could protect the neurons of the hippocampus of AD model animals: Fig. 4 shows the HE staining and Nissl staining results of the CA3 region of the hippocampus from top to bottom, respectively.

The hippocampal CA3 region in the N group was characterized by a substantial quantity of neuronal cells, which were orderly arranged and closely packed.

These cells had a normal structure, distinct edges, and a full appearance. There was a significant presence of Nissl bodies (yellow arrow), with visible nucleoli and distinct nuclear membranes. Upon high magnification, the cytoplasm displayed normal staining. Compared with the N group, the number of neurons AD group was less, the arrangement of pyramidal cells was disordered, the cell body was smaller, the intercellular structure was loose, and there was more pyknosis, deep staining or dissolution of nuclei (red arrow), suggesting that there were more instances of nerve cell necrosis and clear signs of brain aging in mice. Compared with the AD group, the cells in groups D and EA were arranged more orderly, the morphology tended to be normal, and the boundary was obvious. However, there was still obvious nuclear sequestration and deep staining in group D, but in group EA, relatively clear neuronal Nissl bodies could be observed, and nuclear deep staining was not obvious. The number and morphology of cells in the EA group were similar to those in group N. It is suggested that both electroacupuncture and Donepezils can protect neurons in the hippocampal CA3 region of SAMP8 mice and reduce the number of cell damage, but the effect of the EA group was more significant.
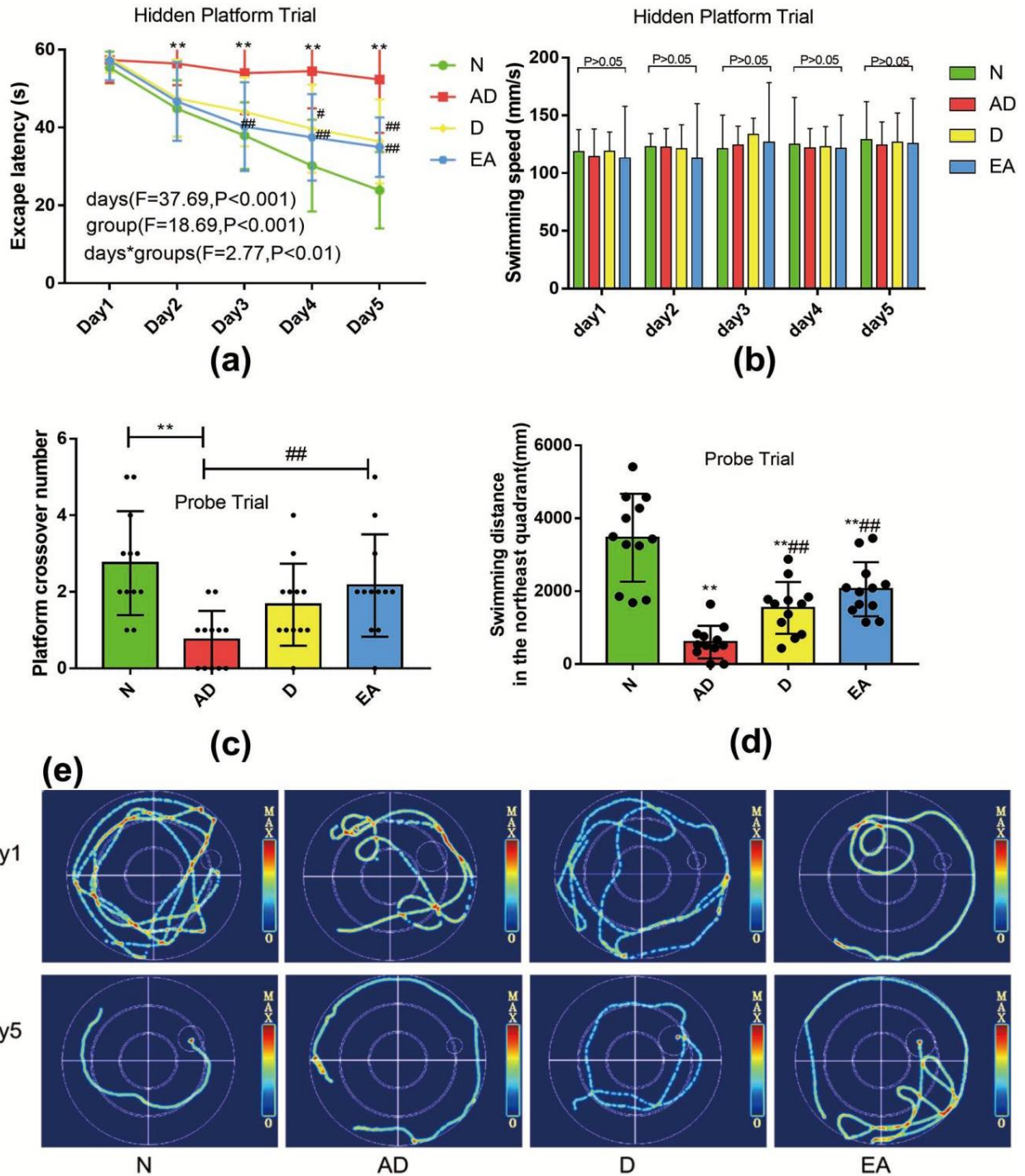

Fig. 2: Morris-water- maze (MWM) experiment Results of MWM trial (n=12) for each group. The platform was kept in the northeast quadrant of the WM pool. (a, b) Comparing the escape latency and speed of swimming of mice of each group in the trial. (c, d) comparing the platform crossover number

and the swimming distance in the target quadrant of each group in the probe trial. (e)Swimming trace of all groups in the hidden platform trial. Compared with N group, *P<0.05, **P<0.01;compared with AD group #P<0.05,##P<0.01;Compared with D group @P<0.05,@@P<0.01,n =12).

(a)

(b)

(c)
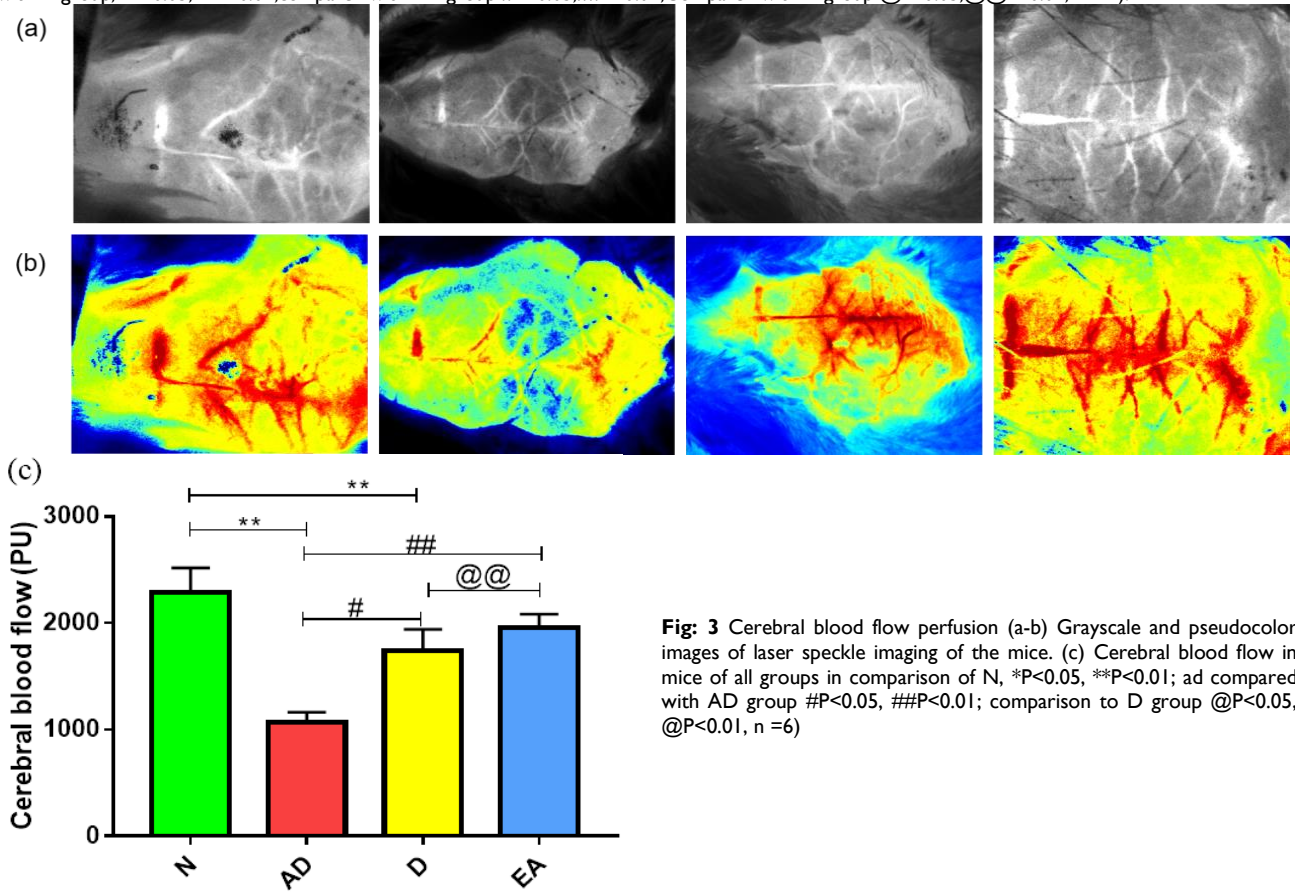
Fig: 3 Cerebral blood flow perfusion (a-b) Grayscale and pseudocolor images of laser speckle imaging of the mice. (c) Cerebral blood flow in mice of all groups in comparison of N, *P<0.05, **P<0.01; ad compared with AD group #P<0.05, ##P<0.01; comparison to D group @P<0.05, @P<0.01, n =6)
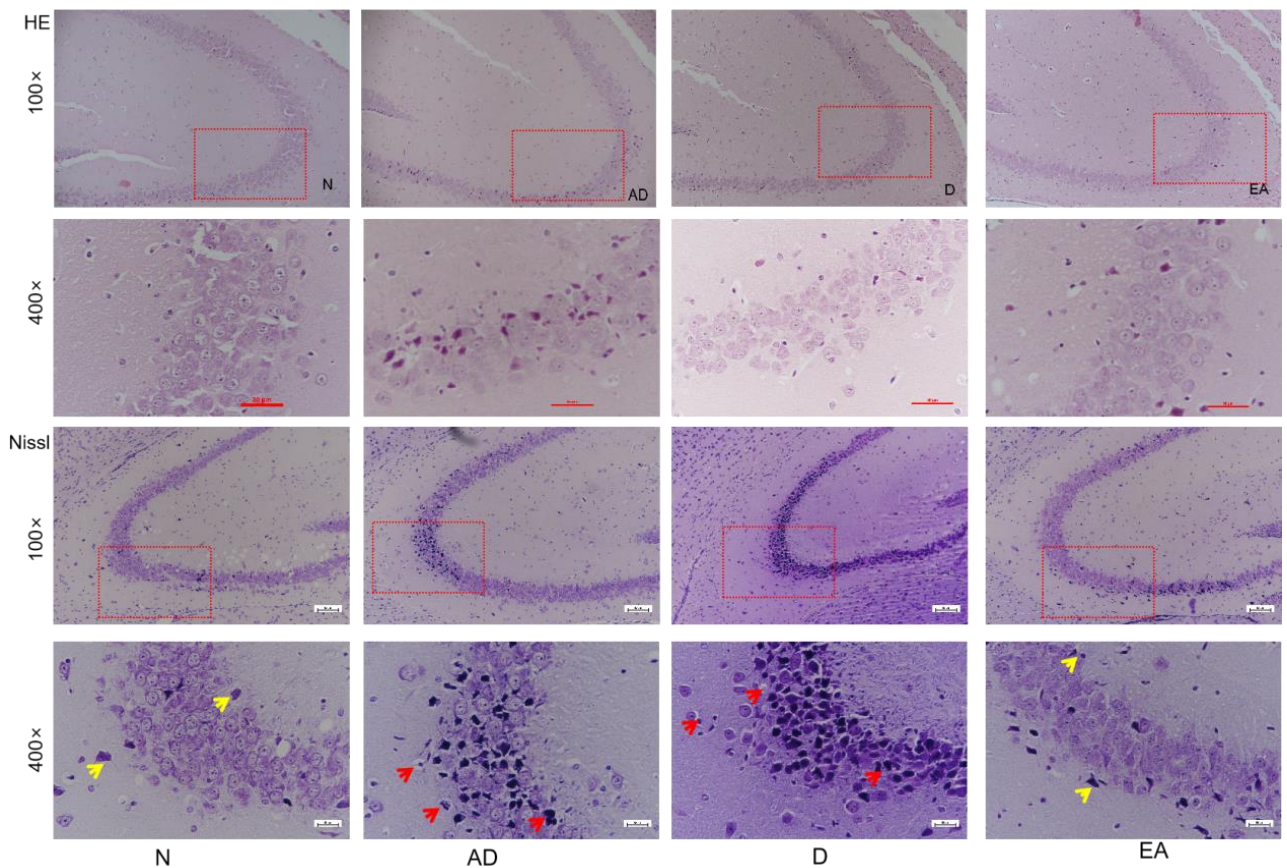
Fig. 4: Nissl and HE stained images of hippocampal CA3. N: Normal group, AD: Alzheimer's disease group, D: Donepezil group, EA: electro acupuncture group. The first and second rows display the HE staining, and the third and fourth rows display the Nissl staining. Neurons containing

Nissl bodies (indicated by the yellow arrow), nerve cells exhibiting edema or karyopyknosis with deep staining (indicated by the red arrow). (Magnification：100× 400×, scale:50um).

EA could enhance the BBB integrity in SAMP8 mice: Moreover, cerebral ischemia also leads to changes in the blood-brain barrier, further aggravating the accumulation of neurotoxic substances such as β -amyloid, leading to the progression of AD. As shown in Fig. 5, compared with Group N, in Group AD: The terminal feet cytoplasm (red arrow) had lower density and severe edema. Mitochondria (purple arrow) had partial membrane dissolution, decreased matrix density, focal edema, and dissolved inner cristae. Capillary endothelial cells (orange arrow) were locally edematous. The basement membrane (yellow arrow) was discontinuous and dissolved. No clear tight junctions between endothelial cells. Compared with Group AD, both Group D and EA improved BBB injury: in Group D, terminal feet had low density and moderate matrix edema. Mitochondria (purple arrow) were highly edematous with membrane dissolution severely decreased matrix density and broken inner cristae. The basement membrane (yellow arrow) was discontinuous and partly dissolved. However, the endothelial cell membrane (orange arrow) was intact, and the tight junction (green arrow) was undamaged. In Group EA, terminal feet had moderate cytoplasmic density and mild edema. Astrocyte terminal feet mitochondria (purple arrow) had a slightly dissolved membrane, moderate matrix density, and no obvious edema but dissolved inner cristae. The endothelial cell membrane (orange arrow) was intact. The tight junction between capillary endothelial cells (green arrow) was damaged. The basement membrane (yellow arrow) had a partial dissolution.

**EA inhibits peripheral serum and central inflammatory reaction of the SAMP8 mice:** The ELISA results of IL-8, TNF- alpha, and IL-10 inflammatory cytokines expressions, in the hippocampus as well as in serum, are presented in Fig. 6. The concentration of serum and the hippocampus of TNF-αand IL-8, in the AD group was higher, however, the IL-10 was lesser than group N mice (P<0.01). When compared to group AD mice, the hippocampal along with serum IL-8 in the EA and D groups decreased. In contrast to the AD group, the contents of IL-8 in the serum and hippocampus of the EA group and D group were significantly decreased. Compared to the group AD, the contents of TNF-alpha and IL-8 in the serum and hippocampus of the EA group were significantly reduced, while the content of IL-10 was significantly enhanced (P<0.01 or P<0.05).

When group AD mice were compared with the group D, they exhibited comparable (P>0.05) alterations in serum levels of TNF-α and IL-10; however, a notable reduction in IL-8 levels was marked (P<0.01). Within the hippocampus, there was a significant decrease in TNF-α and IL-8 levels, alongside a significant (P<0.01 or P<0.05) increase in IL-10 levels. When compared to the N group, the D and EA groups showed significantly elevated levels of IL-8, while IL-10 levels were significantly reduced (P<0.01 or P<0.05). The TNF-α levels in the hippocampus of the D group were higher than those in the N group, with no significant differences noted for other parameters (P>0.05). In comparison to the EA group, the D group had significantly higher IL-8 levels (P<0.01 or P<0.05), a significant decrease in IL-10 levels in the hippocampus, and no significant difference in TNF-α levels (P>0.05). Relative to the N group, both the D and EA groups displayed significantly higher IL-8 levels and significantly lower IL-10 levels (P<0.01 or P<0.05).

**The effect of EA on proteins is related to the formation and disruption of the blood-brain barrier (BBB):** The western blot results of MMP-9, ICAM-1, Occludin, and ZO-1 in the hippocampus are presented in Fig. 7. Compared with those in the N group, the relative expression of MMP-9 and ICAM-1 significantly (P<0.01) increased. At the same time, the secretion of Occludin and ZO-1 significantly decreased in the AD mice group (P<0.05/P<0.01). Both the secretion of MMP-9 and ICAM-1 of the EA and D groups were lower than the AD group (P<0.01), while the relative expression of ZO-1 and Occludin of the EA and D groups were higher than that of

N   AD   D   EA
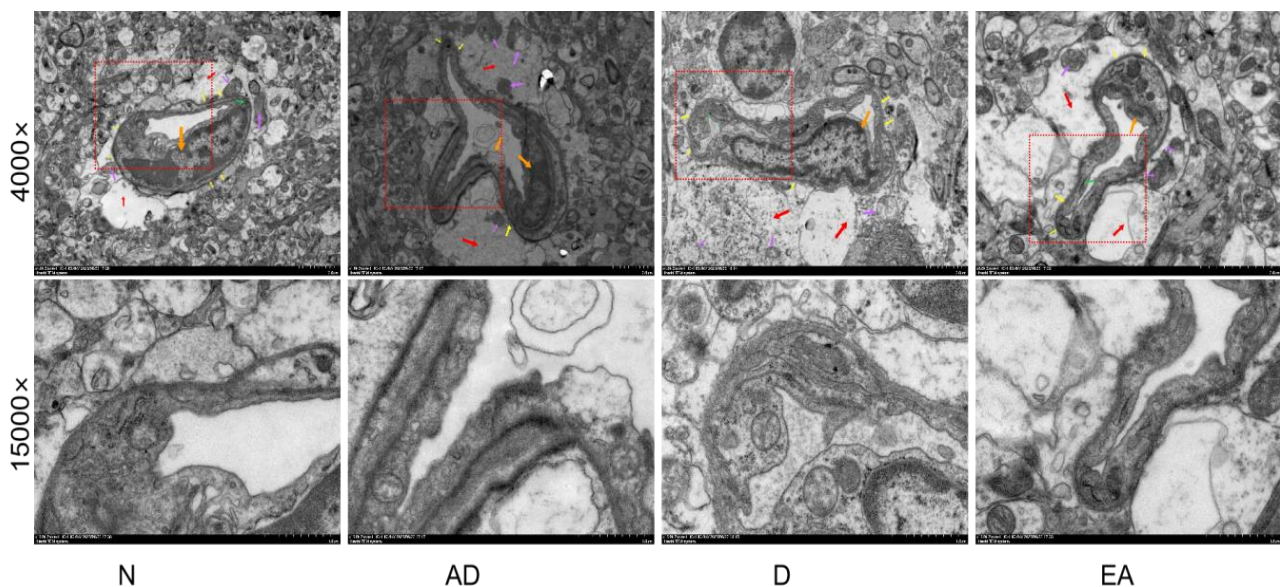
Fig. 5: Transmission Electron Microscopic Observation of the BBB Structure. From left to right are Group N, AD, D, and EA. Magnification:4000×in the first row,15000×in the second row. Astrocyte cytoplasm foot processes (red arrow); mitochondria (purple arrow); capillary endothelial cells (orange arrow); tight junction (green arrow); capillary basement membrane (yellow arrow).
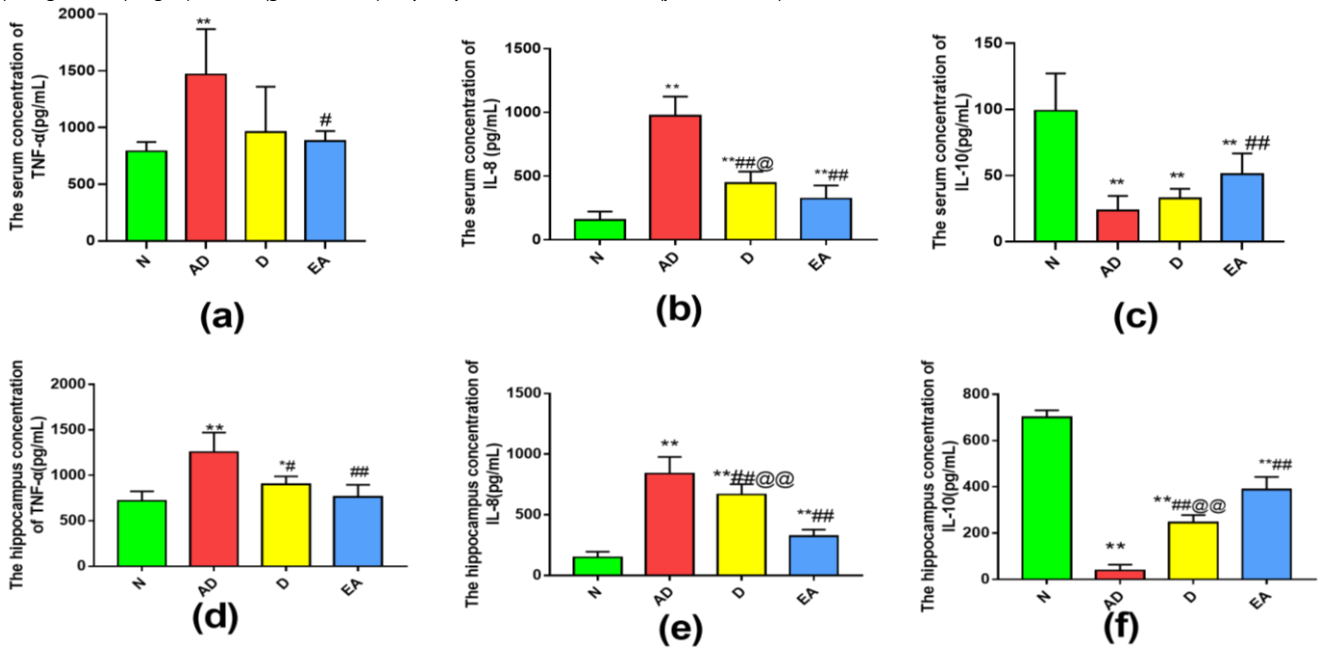
Fig. 6: Expression of cytokines in serum and hippocampus. (a-c): Expression of Inetrleukin-10 Inetrleukin-8 and Tumor necrosis factor-alpha from the serum of the mice of all groups (n=6). (d-f): The expression of IL-10, IL-8 and TNF-a in hippocampus of mice of each group (n=6). Comparison with group N, *P<0.05, **P<0.01; Comparison with AD group, #P<0.05, ##P<0.01; Comparison with D group P<0.05, @P<0.01, each group(n=6).
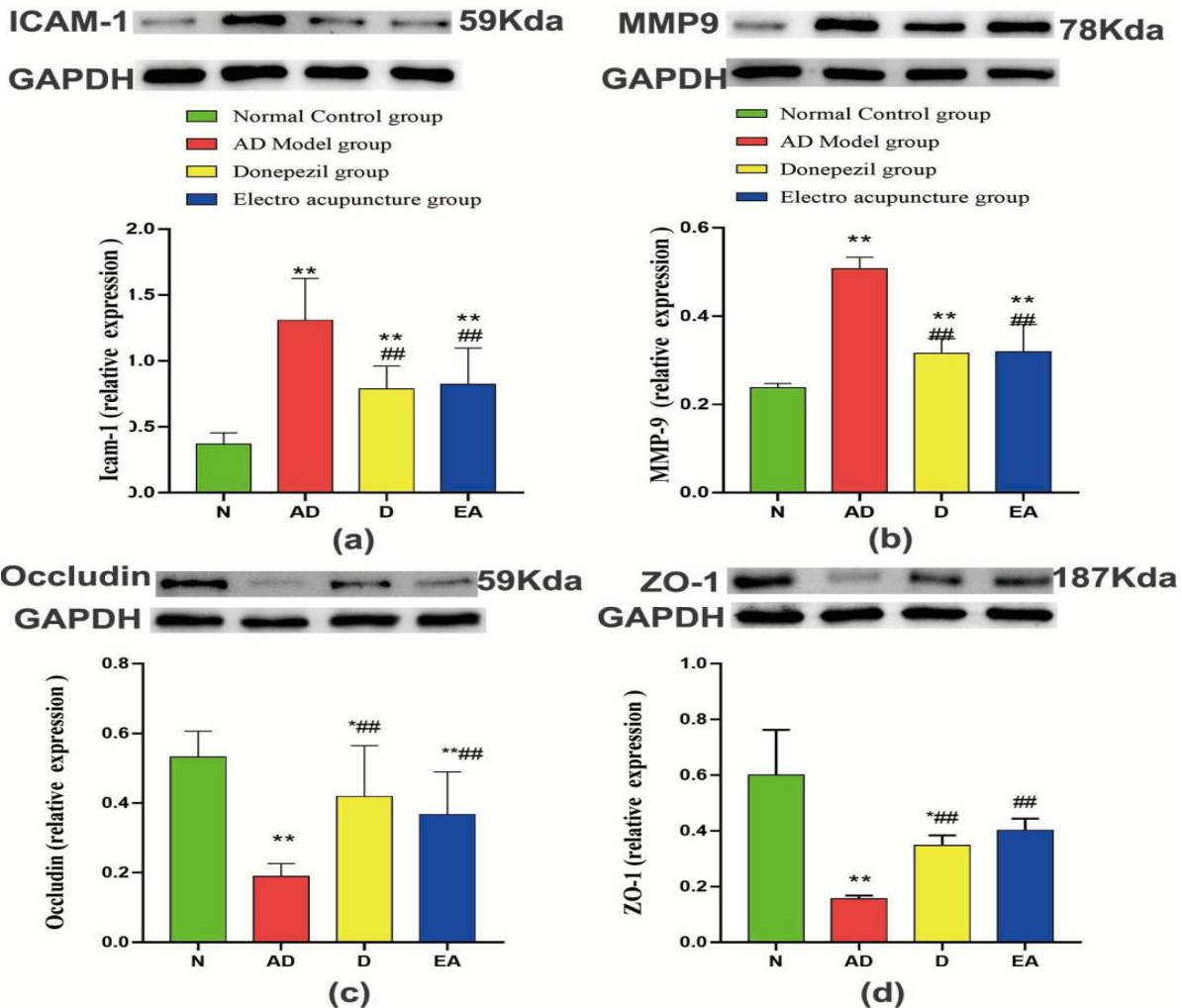
Fig. 7: Disruption and constitution of protein expressions related to the BBB. Comparison of the expression levels of proteins related to the

disruption and constitution of the BBB, along with representative bands of Western Blot. (a-b) Comparison of the relative expression of ICAM-1 and MMP9 (BBB disruption) in each group. (c-d) Comparison of the relative expression of Occludin and ZO-1 (BBB constitution) in each group. Compared with N group, *P<0.05,**P<0.01; compared with AD group <0.05, ##P<0.01; compared with D group P<0.05, @@P<0.01, each group(n=6).

the AD mice (P<0.01, P<0.01). Contents of ICAM-1, and MMP9 in the D and EA group were drastically higher than those in the N group. However, the contents of ZO-1 and Occludin, in the D mice group, and Occludin in the EA group were drastically lower than in mice of group N. Afterward, results were comparable for the EA and D group mice (P>0.05).

DISCUSSION

Along with the excessive deposition of amyloid-βprotein and the hyperphosphorylation of Tau protein, the relationship between insufficient cerebral blood flow (CBF) and the progression of AD has garnered significant attention in recent years, highlighting the critical role of the BBB in maintaining cerebral homeostasis. Current methodologies, including behavioral assessments and advanced imaging techniques, have elucidated the detrimental effects of BBB dysfunction on cognitive decline. CBF of AD is related to the damage of the BBB (Zhang *et al.*, 2022). The BBB plays a crucial role in maintaining the homeostasis of the central nervous system (CNS). The damage to the BBB is considered an early biomarker of AD. The dysfunction of the BBB may lead to the infiltration of toxic substances, such as amyloid-beta protein (Aβ) and tau protein, into the brain, causing inflammation and neurodegenerative changes. At the same time, the dysfunction of the BBB also affects the clearance of brain metabolic waste, thus accelerating the progression of AD. Nevertheless, in AD, the integrity of the BBB is compromised, leading to increased permeability and subsequent neuronal damage. Diseases occur in cases of vascular damage and BBB dysregulation. Vascular pathology is consistent with the underlying mechanisms of aging and AD (Hu and Feng, 2017; Gubskiy *et al.*, 2018; Fang *et al.*, 2023). Cerebral ischemia or chronic cerebral hypoperfusion (CCH) is a common consequence of various cerebrovascular diseases as well as hemodynamic and hematological changes, playing an important role in neurodegenerative diseases and dementia (including vascular dementia and AD), which can lead to cognitive dysfunction. The main causes include vascular structural lesions, changes in cerebral hemodynamics, and alterations in blood components (Zhao and Gong, 2014). In this study, we aimed to investigate the effect of EA on the BBB, CBF, and the cognitive ability of SAMP8 mice, a mouse model of AD.

The Morris-Water-Maze (MWM) assessed spatial memory in AD-related neuropathologies (Tian *et al.*, 2019). Results showed that all groups had comparable swimming speeds (P>0.05), ruling out physical strength bias. Compared to the N group, the behavioral outcomes of the AD group revealed a significantly longer escape latency during days 2 to 5 of the hidden platform trial (P<0.01). Additionally, there was a notable reduction in both the number of platform crossings and the swimming distance within the northeast quadrant during the probe trials (P<0.01). These findings suggest that the SAMP8 mice in the AD group exhibited a substantial deterioration in cognitive memory functions, consistent with the pathological alterations associated with Alzheimer's disease.

EA and donepezil reduced escape latency (P<0.01) and increased swimming distance in the platform quadrant. While both interventions improved spatial memory, only EA significantly increased platform-crossing times compared to the AD group, whereas donepezil showed no significant enhancement (Fig. 2c). Despite comparable statistical outcomes (P>0.05), EA demonstrated earlier latency reduction and higher platform crossings/distance than donepezil, suggesting superior efficacy in restoring learning ability. Trajectory analysis revealed that N, D, and EA groups exhibited purposeful search patterns by day 5, in contrast to the random/marginal trajectories of the AD group (Fig. 2e). These findings align with prior studies (Sun et al., 2021; Li et al., 2025) confirming EA and donepezil's restorative effects on SAMP8 mice's spatial memory.

HE and Nissl staining revealed that there is a large number of neurons in the CA3 region of the hippocampus of SAMP8 mice that are disordered in arrangement, showing signs of neuronal damage such as edema, pyknosis, dark staining of nuclei, and a reduction in Nissl bodies, whereas EA and donepezil reduced neuronal damage. Its pathological manifestations are similar to the trends in water maze behavior.

EA is a combination of traditional acupuncture and electrical stimulation, connecting the acupuncture needles with a pulsed current from an electroacupuncture instrument. This therapy merges traditional hand acupuncture with electrical stimulation by attaching the needle handle to the electroacupuncture therapeutic device and activating the pulsed current to enhance the stimulation of meridian points (Lin *et al.*, 2023). Compared to simple hand acupuncture, electroacupuncture offers advantages such as simpler operation, stable and adjustable stimulation intensity, and a more enduring effect. Given these characteristics, we persist in selecting electroacupuncture as an intervention treatment for studying the mechanisms of AD. In earlier research works, we have found that acupuncture therapies can regulate various pathways in AD, such as regulation of pathological l expressions of Aβ and "Tau" proteins in AD affected areas of brain (Wang *et al.*, 2016; Liao *et al.*, 2024), inhibiting the activation of glial cells and inflammatory responses, and improving peripheral and central thermogenic energy metabolism (Li *et al.*, 2024; Shen *et al.*, 2024.

Cerebral ischemia can induce many mechanisms similar to the pathological manifestations of AD: CCH induces mitochondrial dysfunction and inhibits protein synthesis, disrupting cellular redox balance and leading to oxidative damage. It affects vascular function and neurovascular coupling.─CCH can upregulate β and γ secretase-mediated APP processing, increase Aβdeposition, and accelerate AD pathological changes. In recent years, clinical studies have shown that there is a link between the cumulative reduction of CBF and cognitive decline. CH can independently cause an

increase in plasma phosphorylated tau181 (P-tau181) in patients with AD. After revascularization, the CBF and cognitive function in the brain regions of patients with moyamoya disease have been improved (Zou *et al.*, 2023). Using a laser speckle imaging instrument, we found that compared with the N group, SAMP8 mice exhibited CBF hypoperfusion (P<0.01). Both electroacupuncture (EA) and drug D could increase the CBF perfusion in SAMP8 mice (P<0.01/P<0.05). However, the CBF perfusion in the drug D group was still significantly lower than that in the N mice group (P<0.01). CBF perfusion was comparable between mice of the N group and the EA group mice (P>0.05). Meanwhile, the effect of EA on increasing the CBF perfusion in SAMP8 mice was significantly different from mice of the drug-treated group D (P<0.01). The reasons for these results may be that donepezil primarily inhibits acetylcholinesterase, whereas EA likely acts through multi-target mechanisms, increasing CBF via vascular regulation. reducing inflammation (TNF-α, IL-8) and oxidative stress. Promoting BBB repair via ZO-1/occludin upregulation. This mechanistic divergence is discussed in the Discussion, and we emphasize that the broader effects of EA may explain its advantages in certain outcomes.

Ischemic injury severity correlates with white matter lesion severity, linked to imbalanced inflammatory cytokines and activated glial cells. Cerebral ischemia induces white matter damage via oxidative stress and blood-brain barrier (BBB) disruption (Zhao & Gong, 2014). BBB dysfunction alters the brain microenvironment, reducing cerebral blood flow (CBF) perfusion. For example, ischemic stroke and traumatic brain injury (TBI) trigger BBB breakdown, initiating pathological cascades (e.g., inflammation, oxidative stress, and abnormal angiogenesis) that exacerbate CBF reduction (Hayward et al., 2011; Yao et al., 2023).

To further explore how EA enhances cerebral blood flow, reduces neuronal damage, and improves cognition, we used TEM to observe the BBB structure in each group of mice and detected proteins and cytokines involved in the generation and destruction of the BBB in serum and brain tissue. BBB is primarily composed of Brain microvascular endothelial cells (BMECs) connected through tight junctions (TJ) and adherent junctions (AJ), astrocytes, pericytes, a continuous extracellular basal lamina and extracellular matrix, and neurons, etc. These components function collectively to create a highly selective barrier that safeguards the brain from the penetration of harmful substances. TJs are atretic structures formed by the fusion of the outer layer of the adjacent cell membrane through specific transmembrane proteins. It is located between BMECs and is composed of ZO-1 and Occludins. : Occludin is an important transmembrane protein, located at the two poles of the cell. It has a barrier function and can prevent the lateral diffusion of substances (Virgintino *et al.*, 2004). ZO-1 is located inside the cell, helping to stabilize transmembrane proteins and regulate the structure and function of TJs (Ugalde-Silva *et al.*, 2016). The pericellular pathway regulated by TJs and the transcellular pathway mediated by caveolae can regulate the permeability of BBB. Changes in the distribution and expression level of TJs-related proteins will lead to the opening or closing of

them, thus changing the permeability of BBB (Liu *et al.*, 2012). Astrocyte foot processes are wrapped around the capillary basement membrane, further strengthening the physical barrier function of the blood-brain barrier. Astrocyte foot processes regulate vascular dilation and constriction by releasing molecules like PGE2, AA, and AQP4 (Chu *et al.*, 2014), influencing BBB structure and CBF. Moreover, the expression and distribution of tight-junction proteins and the structural-functional stability of the BBB are regulated by multiple signaling pathways, like MMP9, ICAM-1, and PKC (Mo *et al.*, 2021). Furthermore, the unique extracellular matrix (ECM) of the basement membrane (BM) links endothelial cells to adjacent cells, including astrocytes and pericytes, and the molecular elements of ECM released by these cells offer significant insights into the TJ formation that upholds mature BBB functionality (Yang and Rosenberg, 2015; Yang *et al.*, 2022). Upon over-activation of the inflammatory response, MMP9 is promoted to damage the BBB's basement membrane. Matrix metalloproteinases (MMPs) are a class of zinc-dependent enzymes that dismantle ECM elements in the basement membrane, with MMP-9 believed to play a key role in the degradation of the cerebral BBB (Gubskiy *et al.*, 2018). ICAM-1 absorbs circulating immune cells onto the endothelial cell walls, promotes leukocyte extravasation, activates immune cells to release inflammatory factors, and disrupts the structure and function of the blood-brain barrier (Han and Jiang, 2021).

TEM analysis revealed that AD-group mice exhibited astrocyte/endothelial cell edema, reduced matrix density, mitochondrial/vascular basement membrane disruption, and impaired tight junctions, indicating BBB structural damage. Biochemically, AD mice showed elevated peripheral/hippocampal pro-inflammatory factors (TNF-α, IL-8), MMP9, ICAM-1, and reduced hippocampal TJ proteins (Occludins, ZO-1) and anti-inflammatory IL-10, reflecting systemic and central pro-inflammatory responses linked to BBB dysfunction. Compared to the AD group, both D and EA interventions suppressed pro-inflammatory markers, upregulated TJ proteins, and mitigated BBB injury, demonstrating their protective effects on BBB integrity.

It is a well-established fact in the scientific community that the BBB serves as a vital barrier, effectively restricting the passage of neurotoxic substances from the bloodstream into the brain. However, in AD, BBB pathological changes disrupt the endothelial cell basement membrane and TJs. This allows plasma proteins like fibrin and IgG to infiltrate the CNS, triggering neuroinflammatory responses (Matsuo and Nshihara, 2024). This inflammatory response not only affects the central nervous system but may also interact with the peripheral immune system, further exacerbating the disruption and dysfunction of the BBB (Lee and Funk, 2023). This view is also consistent with the high expression of pro-inflammatory substances detected in the serum and hippocampus of the AD group in this study. Both mitochondrial dysfunctions in the endothelial cells of the BBB and the reduction of tight junctions (TJs) will further lead to an increase in BBB permeability and dysfunction (Zlokovic *et al.*, 2010). These changes further lead to a reduction in cerebral blood flow, affecting the

normal metabolism and energy supply of the brain (Cai *et al.*, 2018). Ultrastructural changes in the capillary wall can cause alterations in the structure of transport proteins, thereby affecting the trans-BBB transport of nutrients (Korczyn, 2015). Cerebral blood flow can be regulated by pericytes in microvessels. During the cerebral ischemia-reperfusion stage, pericytes contract, leading to reduced blood flow, which in turn causes pericyte death and degeneration. This is similar to the pericyte degeneration in neurodegenerative diseases such as Alzheimer's disease (AD). Meanwhile, BBB dysfunction also leads to abnormal cerebral hemodynamics and a decrease in the density of micro vessels. These changes may cause hypoxia and insufficient energy metabolism in brain tissue, thereby exacerbating neurodegeneration (Rani *et al.*, 2023).

The blood-brain barrier (BBB) has a complex structure and function. This study only assesses BBB damage by observing the basement membrane of endothelial cells and intercellular tight-junction proteins, which have limitations. Cerebral blood-flow perfusion is regulated by multiple complex mechanisms, with inflammation-mediated vascular injury being one of them. Pericytes and astrocytic end-feet are key BBB components. How end-feet interact with pericytes to maintain the BBB and regulate blood flow, and their roles in regulating BBB function and improving cerebral blood flow, future work should incorporate glial-specific markers to elucidate their role in EA-mediated BBB protection.

The findings show a significant link between molecular mechanisms and phenotypic outcomes in AD and with EA. In SAMP8 mice, EA-treated ones had better cognitive abilities and CBF. This implies that neuroprotective and anti-inflammatory molecular pathways are key in AD-related deficits. Laser speckle imaging shows that CBF is enhanced in the EA group, suggesting molecular regulation of vascular function, vital for neuronal health. This may restore BBB integrity, as seen by electron microscopy. EA may lower inflammatory cytokine levels, reducing neuroinflammation in AD. Nissl and HE staining show that EA has neuroprotective effects on hippocampal neurons. The link between increased CBF, less inflammation, and better neuronal integrity highlights the complex interplay between molecular and phenotypic aspects in AD. The study assessed outcomes immediately post-intervention (3 weeks).EA's therapeutic potential may be in modulating these molecular pathways for better cognitive and neuronal health. However, long-term effects were not evaluated. We will acknowledge this limitation. Future studies should investigate whether EA's benefits persist over extended periods or require sustained treatment. The causal relationship between the high incidence of cognitive impairment and the expression of brain inflammatory markers remains inconclusive. To strengthen this, we propose future studies using inflammatory pathway inhibitors (e.g., MMP-9 knockouts) to isolate causality.

Conclusions: This study demonstrates that electroacupuncture is capable of effectively ameliorating cerebral blood perfusion insufficiency in AD mice, attenuating the impairment of the blood-brain barrier caused by inflammatory responses, and promoting the expression of CBF proteins. Consequently, they protect brain neurons and enhance the memory and cognitive functions of mice. These results furnish significant experimental evidence for further investigations into the pathogenesis and therapeutic strategies of AD. Future work should incorporate glial-specific markers to elucidate their role in EA-mediated BBB protection. This study acknowledges limitations in assessing long-term effects and causal links between cognitive impairment and neurons. Future studies should focus on astrocyte-mediated central immune regulation to explore the underlying mechanisms of electroacupuncture, thus facilitating the development of more efficacious AD treatment regimens.

REFERENCES

Botella Lucena P and Heneka MT, 2024. Inflammatory aspects of Alzheimer's disease. Acta Neuropath 148(1):31.

Cai Z, Qiao P-F, Wan C-Q et al., 2018. Role of Blood-Brain Barrier in Alzheimer's Disease. J Alzheim Dis 63(4):1223-1234.

Chu H, Ding H, Tang Y et al., 2014. Erythropoietin protects against hemorrhagic blood–brain barrier disruption through the effects of aquaporin-4. Lab Investig 94(9):1042-1053.

Dai J, Gao J and Dong H, 2024. Prognostic relevance and validation of ARPC1A in the progression of low-grade glioma. Aging 16(14):11162-11184.

Ding N, Jiang J, Tian H et al., 2020. Benign regulation of the astrocytic phospholipase A(2)-Arachidonic Acid pathway: The underlying mechanism of the beneficial effects of manual acupuncture on CBF. Front NeuroSci 13:1354-1354.

Fang Y-C, Hsieh Y-C, Hu C-J et al., 2023. Endothelial dysfunction in neurodegenerative diseases. Int J Mol Sci 24(3):2909.

Feng D, Li P, Xiao W et al., 2023. N-methyladenosine profiling reveals that Xuefu Zhuyu decoction upregulates METTL14 and BDNF in a rat model of traumatic brain injury. J Ethanopharmacol 317:116823.

Gubskiy IL, Namestnikova DD, Cherkashova EA et al., 2018. MRI Guiding of the middle cerebral artery occlusion in rats aimed to improve stroke modeling. Translat Stroke Res 9(4):417-425.

Han L and Jiang C, 2021. Evolution of blood-brain barrier in brain diseases and related systemic nanoscale brain-targeting drug delivery strategies. Acta Pharmac Sinica B 11(8):2306-2325.

Hayward NMEA, Tuunanen PI, Immonen R et al., 2011. Magnetic resonance imaging of regional hemodynamic and cerebrovascular recovery after lateral fluid-percussion brain injury in rats. J Cereb Blood Flow Metabol 31(1):166-177.

Hu R and Feng H, 2017. Lenticulostriate Artery and Lenticulostriate-artery Neural Complex: New concept for intracerebral hemorrhage. Curren Pharmacet Design 23(15): 2206-2211.

Huang H, Liao Y, Yu Y et al., 2024. Adult-onset neuronal ceroid lipofuscinosis misdiagnosed as autoimmune encephalitis and normal-pressure hydrocephalus: A 10-year case report and case-based review. Medicine 103(43):e40248-e40248.

Kacířová M, Zmeškalová A, Kořínková L et al., 2020. Inflammation: major denominator of obesity, Type 2 diabetes and Alzheimer's disease-like pathology? Clinic Sci 134(5):547-570.

Korczyn AD, 2015. Vascular parkinsonism-characteristics, pathogenesis and treatment. Nat Rev Nerol 11(6):319-326.

Lee RL and Funk KE, 2023. Imaging blood-brain barrier disruption in neuroinflammation and Alzheimer's disease. Front Aging NeuroSci 15:1144036-1144036.

Li T, Zhang L, Cheng M et al., 2024. Metabolomics integrated with network pharmacology of blood-entry constituents reveals the bioactive component of Xuefu Zhuyu decoction and its angiogenic effects in treating traumatic brain injury. Chin Med 19(1):131-131.

Li Y-Y, Zhou L-W, Qian F-C et al., 2025. scImmOmics: a manually curated resource of single-cell multi-omics immune data. Nucleic Acid Res 53(D1):D1162-D1172.

Liao J, Duan Y, Liu Y et al., 2024. Simvastatin alleviates glymphatic system damage via the VEGF-C/VEGFR3/PI3K-Akt pathway after experimental intracerebral hemorrhage. Brain Res Bullet 216:111045.

Lin Y, Chen C, Ma Z et al., 2023. Emulation of Brain Metabolic Activities Based on a Dynamically Controllable Optical Phantom. Cyborg Bionic System 4:0047-0047.

Liu C, Wu J and Zou M-H, 2012. Activation of AMP-activated protein kinase alleviates high-glucose-induced dysfunction of brain microvascular endothelial cell tight-junction dynamics. Free Rad Biol Med 53(6):1213-1221.

Luan K, Rosales JL and Lee K-Y, 2013. Viewpoint: Crosstalks between neurofibrillary tangles and amyloid plaque formation. Ageing Res Rev 12(1):174-181.

Matsuo K and Nshihara H, 2024. Rebuilding insight into the pathophysiology of Alzheimer's disease through new blood-brain barrier models. Neural Regen Res 19(9):1954-1960.

Mo Y, Yue E, Shi N et al., 2021. The protective effects of curcumin in cerebral ischemia and reperfusion injury through PKC-θ signaling. Cell Cycle 20(5-6):550-560.

Paul D, Agrawal R and Singh S, 2024. Alzheimer's disease and clinical trials. J Basi Clin Physiol Pharmacol 35(1-2):31-44.

Rani S, Dhar SB, Khajuria A et al., 2023. Advanced Overview of Biomarkers and Techniques for Early Diagnosis of Alzheimer's Disease. Cellu Mol Neurobiol 43(6):2491-2523.

Reitz C and Mayeux R, 2014. Alzheimer disease: epidemiology, diagnostic criteria, risk factors and biomarkers. Biochem Pharmacol 88(4):640-651.

Shen B, Xiao S, Yu C et al., 2024. Cerebral hemodynamics underlying ankle force sense modulated by high-definition transcranial direct current stimulation. Cereb Cortex 34(6).

Song Z, Jiang Z, Zhang Z et al., 2024. Evolving brain network dynamics in early childhood: Insights from modular graph metrics. Neuroimage 297:120740.

Sun RQ, Wang ZD, Zhao J et al., 2021. Improvement of electroacupuncture on APP/PS1 transgenic mice in behavioral probably due to reducing deposition of Aβ in hippocampus. Anatom Res 304(11):2521-2530.

Takeda T, Hosokawa M and Higuchi K, 1997. Senescence-accelerated mouse (SAM): A novel murine model of senescence. Experiment Gerontol 32(1-2):105-109.

Tian H, Ding N, Guo M et al., 2019. Analysis of Learning and Memory Ability in an Alzheimer's Disease Mouse Model using the Morris Water Maze. J Visual Experim (152): e60055.

Ugalde-Silva P, Gonzalez-Lugo O and Navarro-Garcia F, 2016. Tight Junction Disruption Induced by Type 3 Secretion System Effectors Injected by Enteropathogenic and Enterohemorrhagic Escherichia coli. Frontiers Cell Infect Microbiol 6:87-87.

Ułamek-Kozioł M, Czuczwar SJ, Januszewski S et al., 2020. Proteomic and Genomic Changes in Tau Protein, Which Are Associated with Alzheimer's Disease after Ischemia-Reperfusion Brain Injury. Int J Mol Sci 21(3):892.

Virgintino D, Errede M, Robertson D et al., 2004. Immunolocalization of tight junction proteins in the adult and developing human brain. Histochemist Cell Biol 122(1):51-59.

Wan H, Zhou S, Li C et al., 2024. Ant colony algorithm-enabled back propagation neural network and response surface methodology based ultrasonic optimization of safflower seed alkaloid extraction and antioxidant. Indust Crop Prod 220:119191.

Wang X, Miao Y, Abulizi J et al., 2016. Improvement of Electroacupuncture on APP/PS1 Transgenic Mice in Spatial Learning and Memory Probably due to Expression of Aβ and LRP1 in Hippocampus. Evid Base Compliment Alter Med: eCAM 2016:7603975-7603975.

Weijie Z, Meng Z, Chunxiao W et al., 2024. Obesity-induced chronic low-grade inflammation in adipose tissue: A pathway to Alzheimer's disease. Ageing Research Reviews 99:102402.

Whitehouse PJ, Price DL, Struble RG et al., 1982. Alzheimer's Disease and Senile Dementia: Loss of Neurons in the Basal Forebrain. Science 215(4537):1237-1239.

Xiao H, Li H, Song H et al., 2020. Shenzao jiannao oral liquid, an herbal formula, ameliorates cognitive impairments by rescuing neuronal death and triggering endogenous neurogenesis in AD-like mice induced by a combination of Aβ42 and scopolamine. J Ethnopharmacol 259:112957.

Yang H, Wang W, Jia L et al., 2020. The Effect of Chronic Cerebral Hypoperfusion on Blood-Brain Barrier Permeability in a Transgenic Alzheimer's Disease Mouse Model (PS1V97L)1. J Alzheim Dis 74(1):261-275.

Yang L, Tao Y, Luo L et al., 2022. Dengzhan Xixin injection derived from a traditional Chinese herb Erigeron breviscapus ameliorates cerebral ischemia/reperfusion injury in rats via modulation of mitophagy and mitochondrial apoptosis. J Ethnopharmacol 288:114988.

Yao Y, Liu F, Gu Z et al., 2023. Emerging diagnostic markers and therapeutic targets in post-stroke hemorrhagic transformation and brain edema. Front Mol NeuroSci 16:1286351-1286351.

Zhang C, Ge H, Zhang S et al., 2021. Hematoma Evacuation via Image-Guided Para-Corticospinal Tract Approach in Patients with Spontaneous Intracerebral Hemorrhage. Neurol Therap 10(2):1001-1013.

Zhang X, Zhu HC, Yang D et al., 2022. Association between cerebral blood flow changes and blood–brain barrier compromise in spontaneous intracerebral haemorrhage. Clinic Radiol 77(11):833-839.

Zhang Y, Zhu L, Li X et al., 2024. M2 macrophage exosome-derived lncRNA AK083884 protects mice from CVB3-induced viral myocarditis through regulating PKM2/HIF-1α axis mediated metabolic reprogramming of macrophages. Redox Biol 69:103016-103016.

Zhao Y and Gong C-X, 2014. From Chronic Cerebral Hypoperfusion to Alzheimer-Like Brain Pathology and Neurodegeneration. Cellu Mol Neurobiol 35(1):101-110.

Zlokovic BV, Deane R, Sagare AP et al., 2010. Low-density lipoprotein receptor-related protein-1: a serial clearance homeostatic mechanism controlling Alzheimer's amyloid β-peptide elimination from the brain. J Neurochem 115(5):1077-1089.

Zou X, Liao Y, Jiang C *et al.*, 2023. Brain perfusion, cognition, and plasma Alzheimer's biomarkers in moyamoya disease. Alzheim Dimentia 19(8):3316-3326.